JOURNAL OF PROPULSION AND POWER
Vol. 15, No. 1, January–February 1999

# Flutter Analysis of Cascades Using an Euler/Navier–Stokes Solution-Adaptive Approach

C. J. Hwang* and J. M. Fang†
*National Cheng-Kung University, Tainan 70101, Taiwan, Republic of China*

**In this study, cascade flutter analyses for inviscid and viscous flows are presented. In the present time-domain approach, the structural model equations for each blade as a typical section having plunging and pitching degrees of freedom are integrated in time by the explicit four-stage Runge–Kutta scheme. A solution-adaptive finite volume method with globally/rigid-deformable dynamic mesh treatments is introduced to solve the two-dimensional Euler/Navier–Stokes equations. For viscous flows, the Baldwin–Lomax turbulence model and two transition formulations are adopted. By comparing with the related data in two inviscid transonic-cascade-flutter problems, the reliability and suitability of the present approach are confirmed. From the time histories of blade displacements and total energy in transonic-flutter calculations, it is observed that the viscous effect has a damping influence on the aeroelastic behavior. The instantaneous meshes and vorticity contours clearly indicate the shock/boundary-layer interaction, large vortex structure, and big plunging motion in the transonic flutter, subsonic stall flutter, and supersonic bending flutter, respectively. By using the fast Fourier transformation and modal identification techniques, the aeroelastic behaviors in the inviscid transonic and viscous transonic, subsonic stall, and supersonic bending flutter problems are further investigated.**

## Nomenclature

$a_\infty$ = freestream speed of sound
$b$ = semichord of the blade
$C_l$ = lift coefficient
$C_m$ = moment coefficient
$C1$, $C2$ = empirical constants for mesh refinement
$c$ = chord length
$E_{\text{tot}}$ = total energy of the blade
$h$ = plunging displacement
$I_\alpha$ = moment of inertia per unit span about the elastic axis
$K_h$ = spring constant for plunging motion
$K_\alpha$ = spring constant for pitching motion
$k_h$ = plunging reduced frequency of the blade, $\omega_h b/U_\infty$
$k_\alpha$ = pitching reduced frequency of the blade, $\omega_\alpha b/U_\infty$
$M_{\text{inlet}}$ = inlet Mach number
$M_\infty$ = freestream Mach number
$m$ = mass of the blade per unit span
$r_\alpha$ = radius of gyration of the blade about the elastic axis in semichord units, $(I_\alpha/mb^2)^{1/2}$
$S_\alpha$ = static moment per unit span about the elastic axis
$T$, $t$ = time
$U_\infty$ = freestream velocity
$V^*$ = reduced velocity, $U_\infty/b\omega_\alpha$
$x_\alpha$ = distance between the elastic axis and center of mass in semichord units, $S_\alpha/mb$
$\alpha$ = pitching displacement
$\Delta W$ = work done on the blade by the aerodynamic loads
$\mu$ = mass ratio of the blade, $m/\pi\rho b^2$
$\rho$ = density of the gas
$\tau$ = nondimensional time, $ta_\infty/2b$
$\omega_h$ = uncoupled plunging natural frequency of the blade, $(K_h/m)^{1/2}$
$\omega_\alpha$ = uncoupled pitching natural frequency of the blade, $(K_\alpha/I_\alpha)^{1/2}$

Received Aug. 11, 1997; revision received Feb. 27, 1998; accepted for publication July 21, 1998. 

*Professor, Institute of Aeronautics and Astronautics, 1 University Road. Senior Member AIAA.

†Graduate Student, Institute of Aeronautics and Astronautics, 1 University Road.

## Introduction

BECAUSE flow-induced vibrations can cause the failure of blades, aeroelastic instability has been mainly considered in the safe design of propfans, compressors, and turbines. Blade vibrations are generally classified into self-excited vibration (flutter)[1] and forced vibration. Although the vibratory motion in both circumstances may cause structure failure, only flutter problems are taken into account in this paper. In two-dimensional cascade flutter calculations,[2–6] the blade/airfoil structure models with an assumption of a typical section[2–5] or having chordwise flexibility[4,6] were introduced. For the typical section model, the section is assumed to be chordwise rigid, where the camber bending is neglected. The pitching and plunging stiffnesses are modeled by torsional and linear springs, respectively, attached at the elastic axis of the typical section. As for the model with chordwise flexibility, a section of unit width in the spanwise direction is allowed to have camber bending. For real turbomachinery blade flutter, the resolution of values for the various two-dimensional parameters is often very problematic. Therefore, the three-dimensional finite element model, such as that given by Bendiksen and Hsiao,[4] was presented. In this work, the typical section model is adopted to evaluate the present two-dimensional solution-adaptive approach by comparing with the related inviscid two-dimensional flutter results.[3,4] In the flutter calculations, with a typical section model, both a frequency-domain[2,3] and time-domain[2–5] analyses have been widely used. For the frequency-domain analysis, the blade displacements are assumed to be a harmonic function of time. Also, the assumption of a linear relation between aerodynamic loads and displacements is made. Therefore, the structural model results in an eigenvalue problem for each blade. It is known that the frequency-domain analysis is valid for small-amplitude oscillations.[2] For the time-domain analysis, no assumption of a linear relation between aerodynamic loads and blade displacements is required. The unsteady equations of motion for the blades and the fluid are integrated simultaneously in time. Therefore, the time-domain analysis can be applied to the cascade flutter with small- and

large-amplitude oscillations. Based on the preceding discussion, the time-domain analysis is employed in this work.

In many aeroelastic instability problems, nonlinear dynamics are important. Several time-marching methods have been developed to investigate the linear and nonlinear flutter phenomena. To understand the features of time-marching methods in the cascade flutter analyses, the following papers are studied. By solving the full-potential equation, Bakhle et al.[2] used the time-domain and frequency-domain methods for linear flutter analyses of two-dimensional cascades. For the two examples, where a cascade with nine blades and a cascade with five blades were considered, respectively, the comparison revealed good agreement between the flutter results from those two methods. Based on an Euler solver, the frequency-domain and time-domain approaches were presented by Reddy et al.[3] For a cascade with five blades, the flutter results obtained from the frequency-domain approach agreed well with the previously published results. When the time-domain approach was used, the expected trends of flutter were achieved. Bendiksen and Hsiao[4] introduced a time-domain approach and an energy point of view to study the aeroelastic stability of two-dimensional cascades and quasi-three-dimensional rotors. In their approach, where finite volume and finite element methods were used, a number of important advantages were described. The flutter results indicated that the transonic flutter problems associated with those cascades and turbomachinery rotors were nonlinear. When the turbomachines operate at off-design conditions, flow separation may happen. The viscous effects should be considered in the flutter analysis of cascades. By using a scheme based on a modified form of the vortex method, Sisto et al.[5] studied the stall flutter phenomenon for incompressible flow past a cascade of airfoils, where the airfoils were modeled structurally as single-degree-of-freedom linear oscillators. They showed that a study of the two-degrees-of-freedom case is mandatory because the practical manifestation of a stall flutter in cascade occurs with a coupled bending-torsion mode. Direct solutions of the unsteady Navier–Stokes equations may be utilized in place of the vortex method.[5] Based on the aforementioned discussion, the inviscid and viscous cascade flutter problems with a coupled bending-torsion mode are investigated. The solution-adaptive approach,[7] which was accurate and suitable for studying the unsteady inviscid flows with complex geometeries and moving boundaries, is used to solve the Euler equations, first. Then, this approach is modified and extended to solve the Navier–Stokes equations.

The objective of this work is to investigate the inviscid and viscous flutter behaviors of cascades. In the present time-domain analysis, the two-dimensional Euler/Navier–Stokes equations and the structural model equations, where each blade is treated as a typical section having plunging and pitching degrees of freedom, are integrated simultaneously in time. By using the explicit four-stage Runge–Kutta scheme, the structural model equations are solved. In the computations of the inviscid flow problems, a solution-adaptive finite volume method[7] is adopted. When the viscous flows are studied, this method is incorporated with a rigid-deformable dynamic mesh algorithm and a treatment of numerical viscous flux function.[8] To predict the onset and extent of transition and include the turbulent effect, two transition models[9,10] are coupled with the Baldwin–Lomax turbulence model.[11] In this work, two inviscid transonic flutter calculations are first performed to understand the inviscid flutter phenomena and accuracy or suitability of the present approach. Later, the viscous transonic, subsonic stall, and supersonic bending flutter problems are investigated.

## Aerodynamic Model

In this work, the two-dimensional unsteady Euler/Navier–Stokes equations with moving cell effects[7,8] are solved in the Cartesian coordinate system. In the viscous flow calculations, an algebraic eddy-viscosity turbulent formulation is adopted.[11] For the transition region that exists between a laminar and turbulent flow, the transition location and intermittency factor are accounted for. The formulations, which were predicted by Abu-Ghannam and Shaw[9] for the natural transition in an attached flow and given by Mayle[10] for the transition in the separated flow, respectively, are used. In the inviscid flow calculations, the locally implicit cell-centered finite volume total variation diminishing (TVD) solution-adaptive approach, which was implemented on the static or dynamic quadrilateral–triangular meshes by Hwang and Fang,[7] was employed. For this scheme, the spatial discretization is treated by a non-MUSCL-type symmetric TVD formulation. The time integration is accomplished by a locally implicit approach, which includes a two-parameter ($\theta$ and $\beta$) expression, Taylor series expansion, and a modified Gauss–Seidel method. In the present computations, the parameters $\theta$ and $\beta$ are chosen to be 1/2 and 0, respectively, and the scheme becomes second-order accurate in time. When the viscous flutter problems are studied, the previously mentioned solution-adaptive approach is coupled with a numerical viscous flux formulation.[8] For this formulation on the quadrilateral–triangular meshes, the first-order derivatives of the velocity components and temperature are calculated by constructing auxiliary cells and using the Green's theorem for surface integration.

In the present flutter calculations, the blade displacements [$\alpha$, ($h/c$)] are obtained by solving the structural model equations. When the inviscid flutter problems are studied, the globally dynamic mesh algorithm[7] and the values of $\alpha$ and $h/c$ are used to determine the instantaneous positions of grid points on triangular mesh. This kind of dynamic mesh is immediately responded to moving blades. For the viscous flutter problems, the rigid-deformable dynamic mesh algorithm[8] is introduced to maintain the orthogonality on each blade surface and the smoothness of quadrilateral–triangular meshes. With regard to the rigid-deformable dynamic mesh algorithm, a layer of O-typed quadrilaterals, which is generated around each blade surface, is moved and oscillated rigidly with respect to its own blade. Then, the triangles, which are distributed elsewhere, are treated by a dynamic mesh algorithm.[7] In addition to the aforementioned dynamic mesh algorithms, the mesh-refinement technique[7] is employed, so that the meshes can be automatically refined during the present unsteady calculations. For this mesh-refinement technique, a coarse mesh is used as a background grid, and a two-level refinement procedure is employed. In this procedure, the values of $C1$ and $C2$ are chosen to multiply by the average value of the gradient of density, so that two threshold values are determined. In general, the values of $C1$ and $C2$ are dependent on the flow feature and the number of background cells to be refined during the computations. If the values of $C1$ and $C2$ are small, the number of cells is large. Therefore, more computational time is required, but higher resolution is obtained.

During the flutter calculations, the steady-state solutions are chosen as initial conditions. In the steady-state computations, adiabatic wall and no-penetration or no-slip conditions are imposed on the blade surfaces. The pressure and density at the blade surfaces are extrapolated from the values at the interior cells. By giving the freestream Mach number and flow angle, the one-dimensional characteristic analysis based on Riemann invariants is used to treat inlet boundary. At the exit boundary, the back pressure is prescribed, and the other flow properities are extrapolated from those at the interior cells. In the flutter calculations with dynamic mesh effects, the movement of the boundary cells must be taken into account for implementing the boundary conditions. The boundary treatments on the blade surfaces are the same as those in Refs. 7 and 8. At inlet and outlet planes, one-dimensional unsteady nonreflective boundary conditions are employed.[12] In the flutter calculations with an interblade phase angle ($\sigma$) of 180 deg, the symmetric treatment is applied on upper and lower boundaries of the computational domain (Figs. 1a and 1b). As for the spatially periodic boundaries of cascade with multiple blades (Figs. 1c and

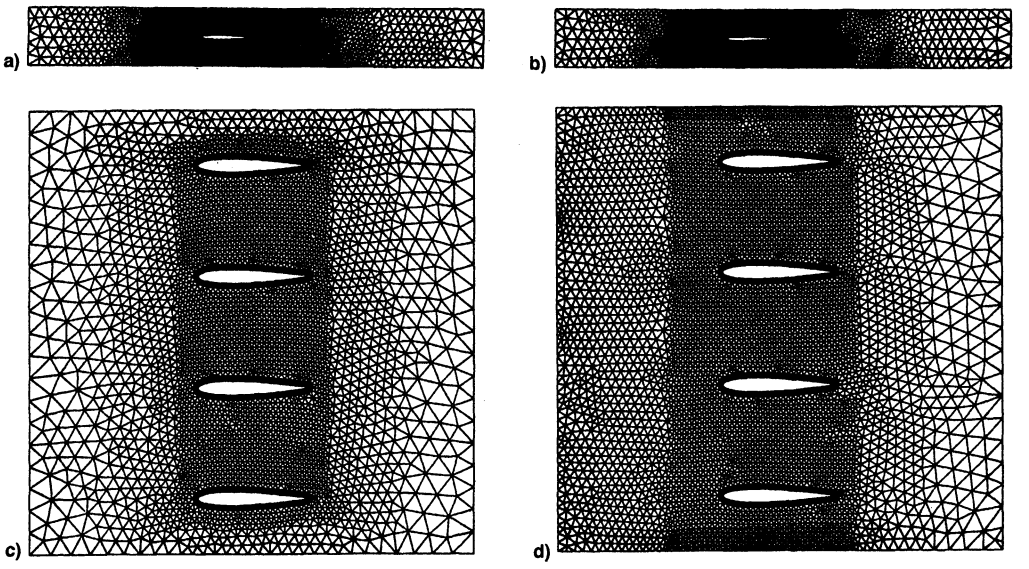


**Fig. 1 Four kinds of coarse meshes (background grids) in the inviscid and viscous flutter calculations: a) inviscid transonic flutter calculation at $M_\infty$ = 0.85 (NACA 0006 cascade), b) viscous transonic flutter calculation at $M_\infty$ = 0.85 (NACA 0006 cascade), c) subsonic stall flutter calculation at $M_\infty$ = 0.3 (NACA 0012 cascade), and d) supersonic bending flutter calculation at $M_\infty$ = 1.1 (NACA 0012 cascade).**

1d), the numerical treatment in steady and unsteady calculations is the same as that in Ref. 8.

## Structural Model

In this paper, each blade of a cascade is modeled as a typical section with plunging ($h$, positive down) and pitching ($\alpha$, postive clockwise) degrees of freedom. The structural damping is not considered in the present calculations. Introducing a nondimensional time $\tau = ta_\infty/2b$, the nondimensional form of equations of motion for each blade becomes

$$[M]\{\ddot{q}\} + [K]\{q\} = \{F\} \tag{1}$$

where

$$[M] = \begin{bmatrix} 1 & \frac{x_\alpha}{2} \\ \frac{x_\alpha}{2} & \frac{r_\alpha^2}{4} \end{bmatrix}, \qquad [K] = \begin{bmatrix} 4M_\infty^2 k_h^2 & 0 \\ 0 & M_\infty^2 r_\alpha^2 k_\alpha^2 \end{bmatrix} \tag{2}$$

$$\{q\} = \begin{Bmatrix} \frac{h}{2b} \\ \alpha \end{Bmatrix}, \qquad \{F\} = \begin{Bmatrix} \frac{-2M_\infty^2 C_l}{\pi\mu} \\ \frac{2M_\infty^2 C_m}{\pi\mu} \end{Bmatrix} \tag{3}$$

In the preceding equations, the dots over $q$ indicate differentiation with respect to time.

By using $V^* = U_\infty/b\omega_\alpha$ as the reduced velocity, the matrix $[K]$ in Eq. (2) can be rewritten as

$$[K] = \begin{bmatrix} \left(\frac{2M_\infty \omega_h}{V^* \omega_\alpha}\right)^2 & 0 \\ 0 & \left(\frac{M_\infty r_\alpha}{V^*}\right)^2 \end{bmatrix} \tag{4}$$

The total energy ($E_{\text{tot}}$) of each blade and work ($\Delta W$) done on the blade by the aerodynamic loads are expressed as

$$E_{\text{tot}} = \tfrac{1}{2}\{\dot{q}\}^T[M]\{\dot{q}\} + \tfrac{1}{2}\{q\}^T[K]\{q\} \tag{5}$$

$$\Delta W = \int \{\dot{q}\}^T\{F\}\, d\tau \tag{6}$$

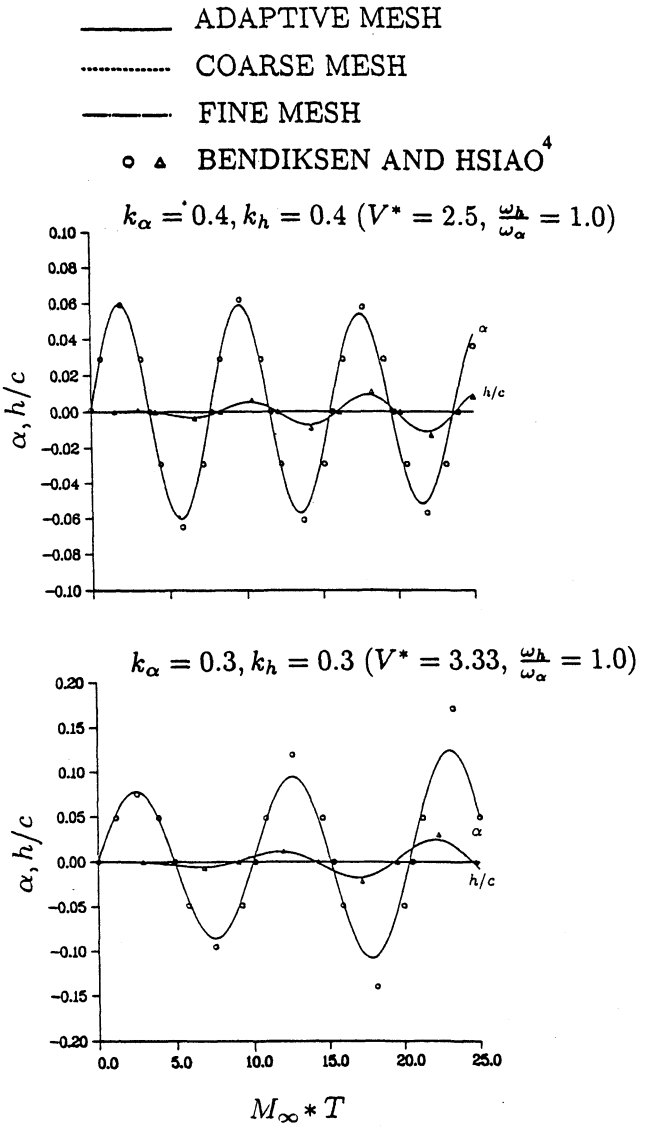


**Fig. 2 Histories of $h/c$ and $\alpha$ for the unstaggered NACA 0006 cascade in inviscid transonic flutter calculations at $M_\infty$ = 0.85.**

As a system is conservative, the difference of $E_{tot}$ and $\Delta W$ should be equal to a constant, i.e., a value of initial energy. In the time-marching solution procedure, Eq. (1) is rewritten into first-order ordinary differential equations. Then, an explicit four-stage Runge–Kutta scheme is applied to obtain the resulting structural displacements. In the present flutter calculations, the steady-state solutions are first obtained by solving the Euler/Navier–Stokes equations. Those steady-state solutions are chosen as the initial conditions, and a blade is given a small pitching velocity. Later, the fluid and structural equations are simultaneously integrated in time, where the aerodynamic loads drive the structural equation and the resulting structural displacements vary the aerodynamic loads.

## Results and Discussion

### Inviscid Transonic Flutter

To evaluate the present approach and investigate the inviscid transonic flutter phenomena, two cascade problems are studied. First, an unstaggered NACA 0006 inviscid transonic cascade flow is computed.[4] The cascade parameters are a cascade gap-to-chord ratio ($s/c$) of 1.0, an interblade phase angle ($\sigma$) of 180 deg, and a mass ratio ($\mu$) of 192 (titanium). On a coarse mesh shown in Fig. 1a, the steady-state solution is obtained, where the exit pressure ratio ($p_e/p_\infty$), freestream Mach number ($M_\infty$), and angle of attack ($\alpha_\infty$) are equal to 1.05, 0.85, and 0-deg, respectively. Given an initial pitching velocity ($d\alpha/d\tau$) of 0.0425, the flutter calculations are processed by using the solution-adaptive approach. At the tenth time-step, the coarse mesh (Fig. 1a) is refined, where $C1$ and $C2$ are chosen to be 4.0 and 12.0, respectively. Later, the automatic mesh-refinement procedure[7] with the same values of $C1$ and $C2$ is adopted. In addition to the previously mentioned calculations on adaptive meshes, the computations on two fixed (coarse and fine) meshes are performed to evaluate the present solution-adaptive approach. As shown in Fig. 2, the time histories of plunging and pitching displacements of the cascade referred to the elastic axis at 38% chord are identical among those computations on three kinds of meshes. For the case with $k_\alpha/k_h$ = 0.3/0.3 ($V^*$ = 3.33, $\omega_h/\omega_\alpha$ = 1.0), the amplitudes of $h/c$ and $\alpha$ progressively grow, so that blade flutter occurs. Except for the amplitude of $\alpha$, the time histories of $\alpha$ and $h/c$ are similar to those in Ref. 4 (Fig. 2). When the value of $k_\alpha/k_h$ is equal to 0.4/0.4 ($V^*$ = 2.5, $\omega_h/\omega_\alpha$ = 1.0), the present solutions compared well with the related results given in Ref. 4, where the amplitudes of $\alpha$ and $h/c$ progressively decay and grow, respectively (Fig. 2). Because the aeroelastic behavior is not clearly understood in this case, the stability of the blade is determined by the analysis of $E_{tot}$ and $\Delta W$. It is known that $E_{tot}$ will increase with time if the blade flutter happens[4]; otherwise, the blade is stable. From the time histories of $E_{tot}$ and $\Delta W$ shown in Fig. 3, the blade flutter occurs for the present two cases. Because the present inviscid flow is a nondissipative system, $E_{tot} - \Delta W$ should be a constant value. As shown in Fig. 3, the values of $E_{tot} - \Delta W$ indicate that the computation on the adaptive mesh is the best among the three kinds of meshes for each case. By using modal identification analysis,[13] damping of the responses can be estimated. Then, the flutter-reduced velocity

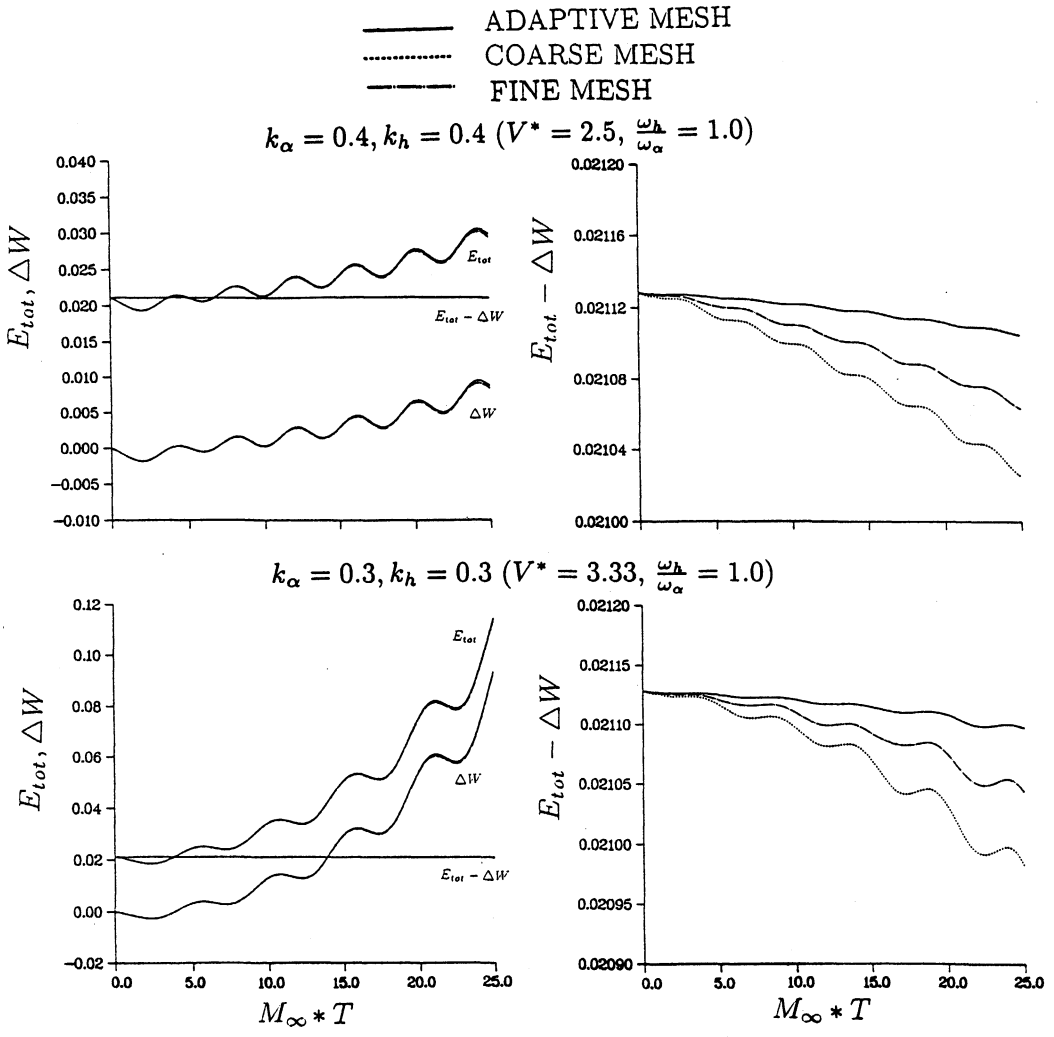


**Fig. 3 Histories of $E_{tot}$, $\Delta W$, and $E_{tot} - \Delta W$ for the unstaggered NACA 0006 cascade in inviscid transonic flutter calculations at $M_\infty$ = 0.85.**

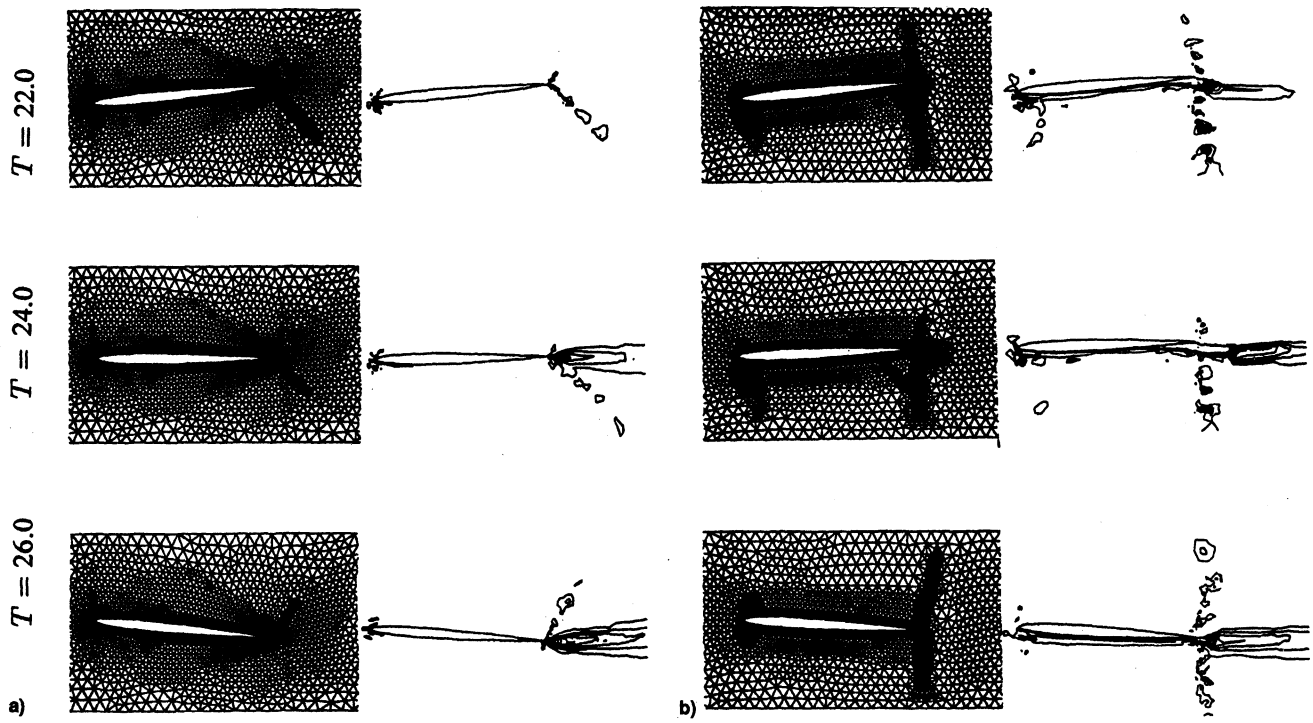


**Fig. 4** Instantaneous meshes and corresponding vorticity contours for the unstaggered NACA 0006 cascade in transonic flutter calculations at $M_\infty = 0.85$ and $V^* = 3.33$: a) inviscid and b) viscous flows.

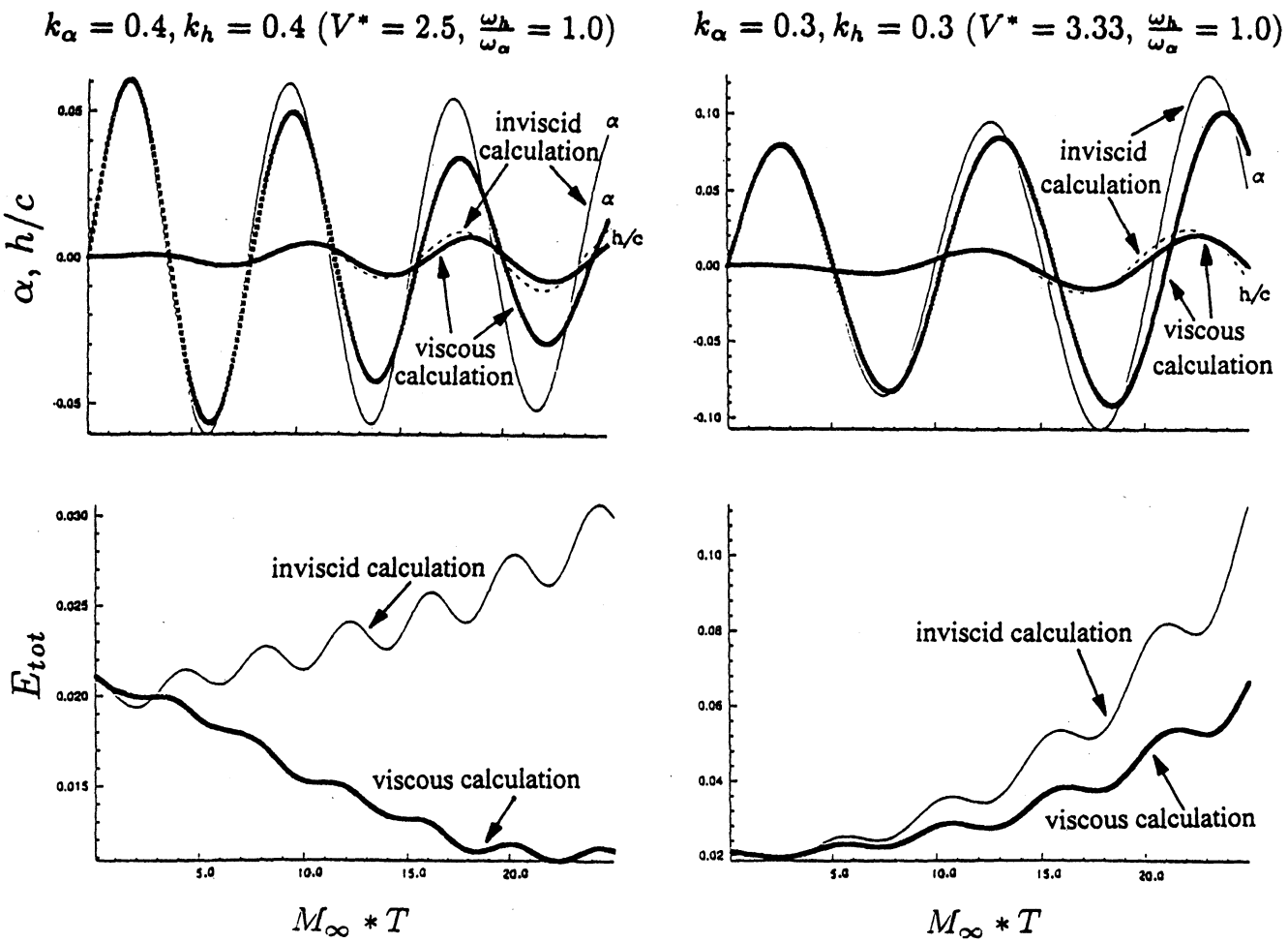


**Fig. 5** Histories of $h/c$, $\alpha$, and $E_{tot}$ for the unstaggered NACA 0006 cascade in inviscid and viscous transonic flutter calculations at $M_\infty = 0.85$.

is defined when the largest damping vanishes. Based on the aforementioned modal identification analysis and an extrapolation process, the flutter-reduced velocity is $V_F^* = 2.3$. In addition to the previously mentioned aeroelastic behavior, it is interesting to study the unsteady inviscid flow phenomena. As shown in Fig. 4a ($V^* = 3.33$, $\omega_h/\omega_\alpha = 1.0$), the time variations of strength and the location of trailing-edge shocks are observed. Also, the vorticity contours are concentrated around the shock, the leading edge, or downstream of the trailing edge. According to the preceding discussion, the present solution-adaptive approach is reliable for studying the cascade flutter problems.

To further understand the suitability of the present approach for a multiple-blade time-accurate calculation, a cascade with five blades is investigated. The geometry, flow conditions, and structural parameters are the same as those presented by Reddy

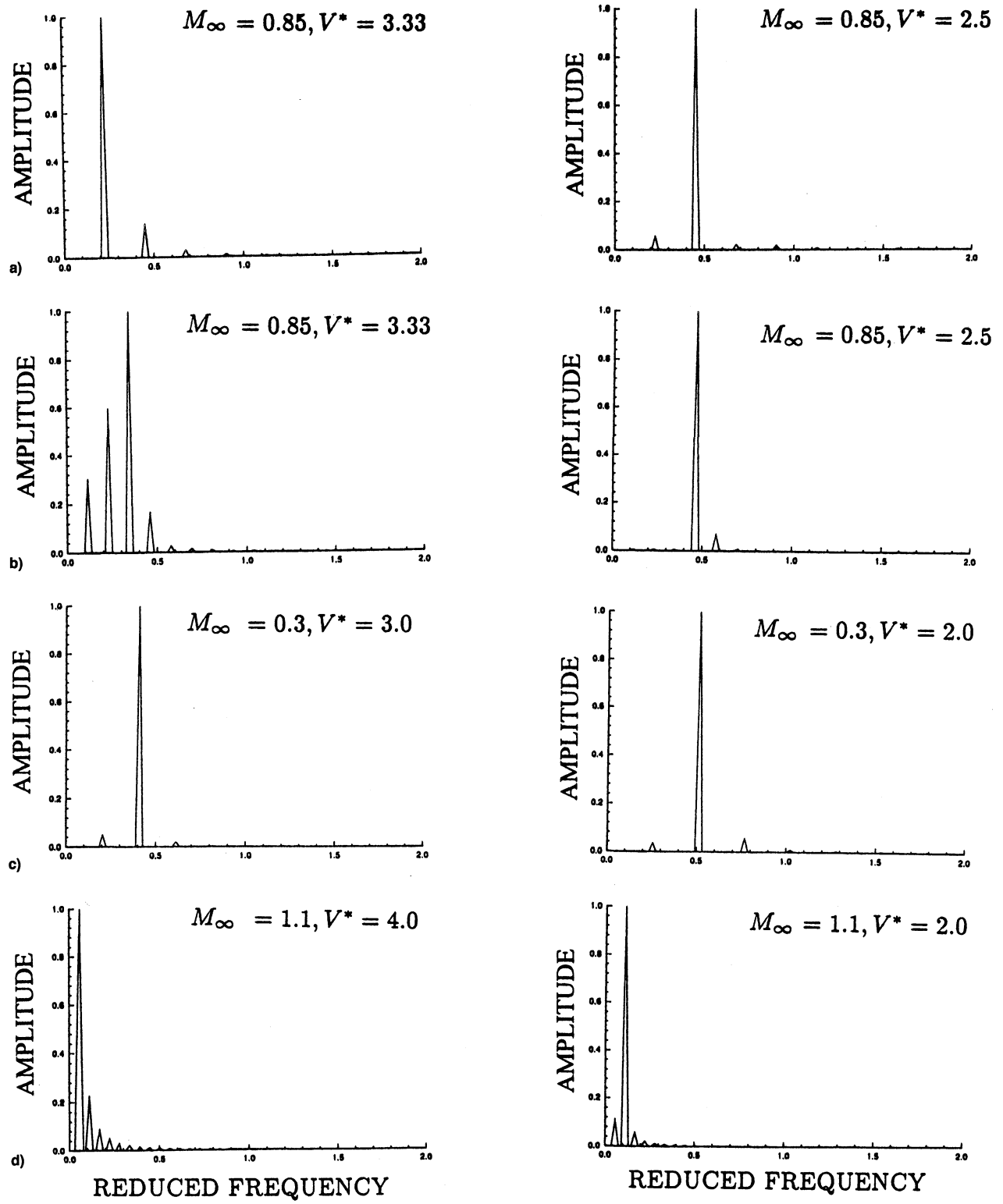


**Fig. 6 FFT of cascade responses for the inviscid and viscous flutter calculations: a) pitching displacement in inviscid transonic flutter calculation, b) pitching displacement in viscous transonic flutter calculation, c) pitching displacement in viscous subsonic stall flutter calculation, and d) plunging displacement in viscous supersonic bending flutter calculation.**

et al.[3] For an inlet Mach number and angle of attack equal to 0.7 and 2.15 deg, respectively, the steady-state solution is obtained, where the outflow static back pressure is adjusted by trial and error until the inlet desired Mach number is matched. The lowest blade is given a small initial pitching velocity ($d\alpha/d\tau$) of 0.0425, and all the other blade displacements and velocities are initially zero. Calculation is performed only for $V^* = 2.0$, and a constant marching time step of $\Delta t = 0.004$ is chosen. During the solution-adaptive calculation, $C1$ and $C2$ are set to be 6.0 and 15.0, respectively. In the fast Fourier transform (FFT) analysis of pitching displacement, the reduced frequency is equal to 0.243, which agrees with the value of 0.25 presented by Reddy et al. According to the preceding discussion, the present solution-adaptive approach is suitable for studying flutter problems with multiple-blade configurations.

**Viscous Transonic Flutter**

In the viscous transonic flutter analysis, the previously mentioned NACA 0006 unstaggered cascade is again adopted. The geometry, flow conditions, and structural parameters are the same as those in the inviscid transonic flutter case. The values of Reynolds number and Courant–Friedrichs–Lewy (CFL) number are equal to $1 \times 10^6$ and 6.0, respectively. In the present solution-adaptive approach, the mesh shown in Fig. 1b is chosen as the background grid, and the values of $C1$ and $C2$ are set to be 0.3 and 0.8, respectively. To investigate the unsteady viscous flow phenomena and compare with the related results in inviscid flow calculations, the instantaneous meshes and corresponding vorticity contours at $T = 22.0$, 24.0, and 26.0 are plotted in Fig. 4b ($V^* = 3.33$). Because of the boundary-layer effect, the shock structure (such as the $\lambda$ shock) and related unsteady behaviors are different from those in inviscid flow. The regions with a high gradient of vorticity are located around the shocks, leading edge, wake, and lower surface of the blade. To understand the aeroelastic behavior, the time histories of $h/c$, $\alpha$, and $E_{tot}$ of the blade are plotted in Fig. 5. For the case with $V^* = 2.5$, the magnitudes of $\alpha$ and values of $E_{tot}$ progressively decay. Therefore, the motion of the blade is stable with time. However, the blade motion for this case in inviscid flow is unstable. When the value of $V^*$ is replaced by 3.33, the blade responses progressively increase, so that blade flutter occurs. The values of $E_{tot}$ and amplitudes of $h/c$ and $\alpha$ in viscous flow are smaller than those in inviscid flow. From the preceding discussion, it is obvious that the viscous effect has a damping influence on the aeroelastic behavior. To further understand the flutter behaviors in inviscid and viscous flows, FFT analysis of the pitching displacements is presented in Figs. 6a and 6b. For those two unstable cases with $V^* = 3.33$, the reduced frequency of fundamental instability ($f_0$) in viscous flow is a value of 0.346 (Fig. 6b), whereas the value of $f_0$ is equal to 0.225 (Fig. 6a) in inviscid flow. It is interesting and worthwhile to indicate that the distributions of normalized amplitude of pitching displacement are significantly different from each other. In the inviscid flutter calculation (Fig. 6a; $V^* = 3.33$), the magnitudes of first ($2f_0$), second ($4f_0$), and higher harmonics are much smaller than that of the fundamental instability. Therefore, the aeroelastic behavior of inviscid flutter is mainly determined by the fundamental instability. When the viscous flutter problem (Fig. 6b; $V^* = 3.33$) is studied, the magnitude of frequency $2f_0/3$ is significant, so that the flutter behavior is not completely dominated by the fundamen-

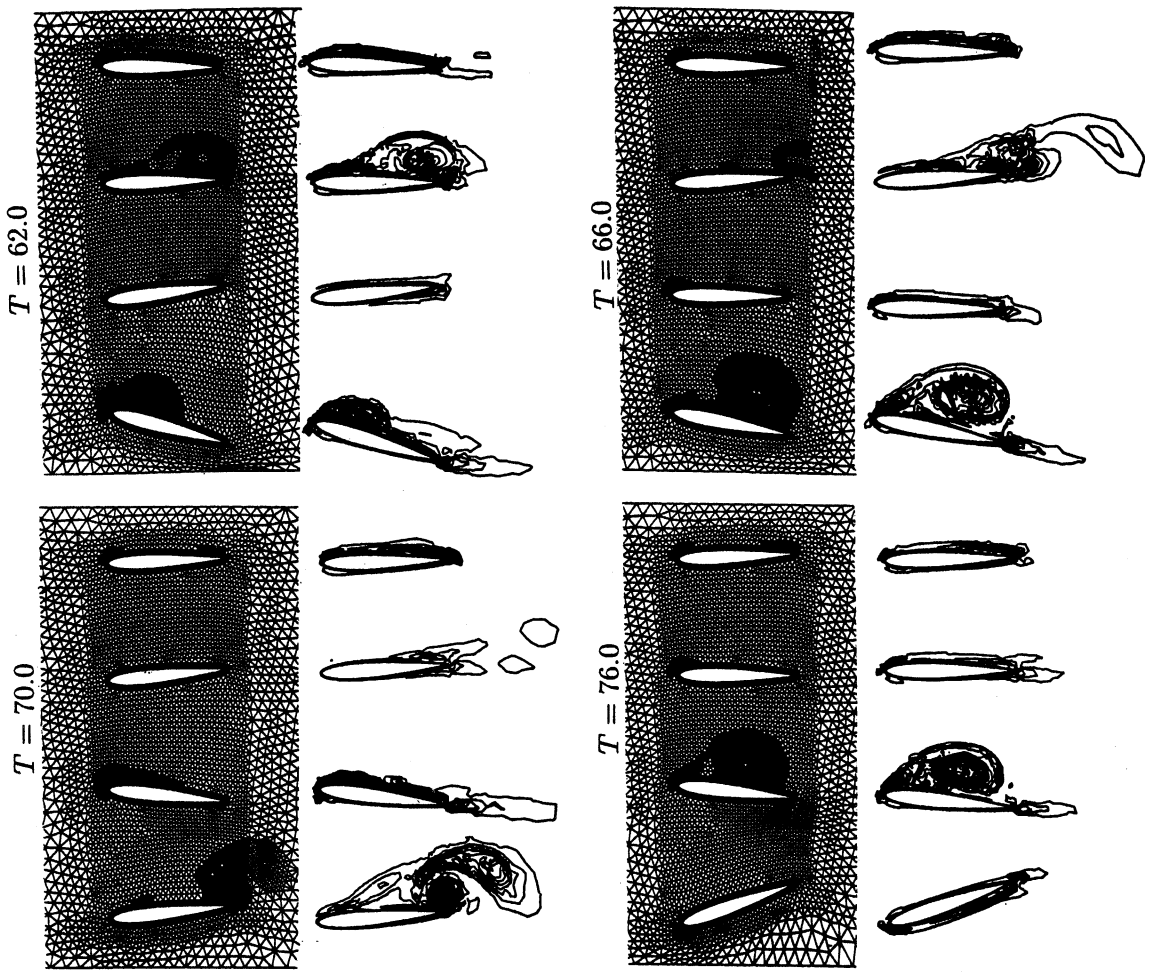


**Fig. 7 Instantaneous meshes and corresponding vorticity contours for the unstaggered NACA 0012 cascade in viscous subsonic stall flutter calculations at $M_\infty = 0.3$ and $V^* = 3.0$.**

tal instability. With regard to stable (viscous flow) and unstable (inviscid flow) cases with $V^* = 2.5$, the value of fundamental frequency ($f_0$) in viscous flow is equal to 0.464 (Fig. 6b), which is closer to that of 0.451 (Fig. 6a) in inviscid flow. Also, the distributions of normalized amplitude of pitching displacement indicate that the aeroelastic behaviors in viscous and inviscid flows are controlled by the fundamental instability. Based on the modal identification analysis and an interpolation process, the flutter reduced velocity is $V_F^* = 2.94$, which is higher than that in the inviscid flutter calculation ($V_F^* = 2.3$). According to the aforementioned discussion, it is concluded that the viscous effect should be considered in the cascade flutter analysis.

### Viscous Subsonic Stall Flutter and Viscous Supersonic Bending Flutter

To further understand the different kinds of cascade flutter behavior, the subsonic stall and supersonic bending flutter problems are investigated by the present solution-adaptive approach. For those two kinds of flutter problems, the computational domain comprises four NACA 0012 blades (Figs. 1c and 1d), where the gap-to-chord ratio and stagger angle are the values of 1.0 and 0 deg, respectively. The structural parameter values are $r_\alpha = 0.5$, $x_\alpha = 0.25$, $\omega_h/\omega_\alpha = 0.2$, $\mu = 100$, and the elastic axis at 25% chord. The values of Reynolds and CFL numbers are equal to $9 \times 10^6$ and 3.0, respectively. By applying the mesh-refinement procedure to the present flutter calculations, $C1$ and $C2$ are set to be 0.3 and 0.8, respectively. For each kind of flutter calculation, the lowest blade is given a small initial pitching velocity ($d\alpha/d\tau$) of 0.0425, and all the other blade displacements and velocities are initially zero.

In the subsonic stall flutter analysis, the steady-state calculation on a coarse mesh (Fig. 1c) is performed at a freestream Mach number $M_\infty = 0.3$, angle of attack $\alpha_\infty = 22$ deg, and the outflow static back pressure ratio $p_e/p_\infty = 1.05$. For two kinds of reduced velocities $V^* = 2.0$ and 3.0, the coarse mesh (Fig. 1c) is used as a background grid during the solution-adaptive calculations. After $T \geq 50.0$, the coarse mesh is refined according to the unsteady solutions. For the case with $V^* = 3.0$, the instantaneous meshes and corresponding vorticity contours (Fig. 7) clearly indicate the formation/convection/shedding of vortices along the lowest, second, and third blade surfaces. The time-variation of vorticity contours around the fourth blade is less significant. To understand the aeroelastic behavior, time histories of $h/c$, $\alpha$, and $E_{tot}$ of the lowest blade are plotted in Fig. 8. For the case with $V^* = 3.0$, the amplitudes of $\alpha$ progressively increase. The stall flutter is triggered by the motion of the lowest blade. Considering the case with $V^*$ equal to 2.0, the histories of $\alpha$ and $E_{tot}$ indicate that the lowest blade is nearly neutrally stable. From the FFT output of pitching displacement (Fig. 6c), the reduced frequency of fundamental instability ($f_0$) is equal to 0.409 when the unstable case with $V^* = 3.0$ ($k_\alpha = 0.333$) is studied. The subsonic stall flutter behavior is dominated by the fundamental instability in this example. For the case with $V^* = 2.0$ ($k_\alpha = 0.5$), the value of fundamental frequency ($f_0$) is equal to 0.511 (Fig. 6c), which is close to the value of $k_\alpha$. Similar to the case with $V^* = 3.0$, the aeroelastic behavior is controlled by the fundamental instability. Based on the modal identification analysis and an interpolation process, the flutter reduced velocity is found to be 2.19.

Finally, a supersonic bending flutter analysis is presented for the same cascade structure. When the freestream Mach number, angle of attack, and outflow static back pressure ratio are

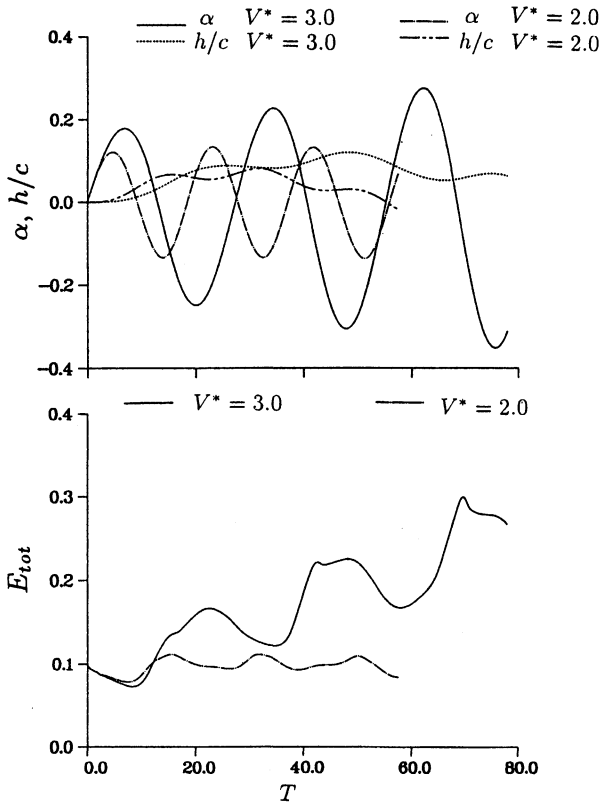


**Fig. 8 Histories of $h/c$, $\alpha$, and $E_{tot}$ for the lowest blade of an unstaggered NACA 0012 cascade in viscous subsonic stall flutter calculations at $M_\infty = 0.3$.**

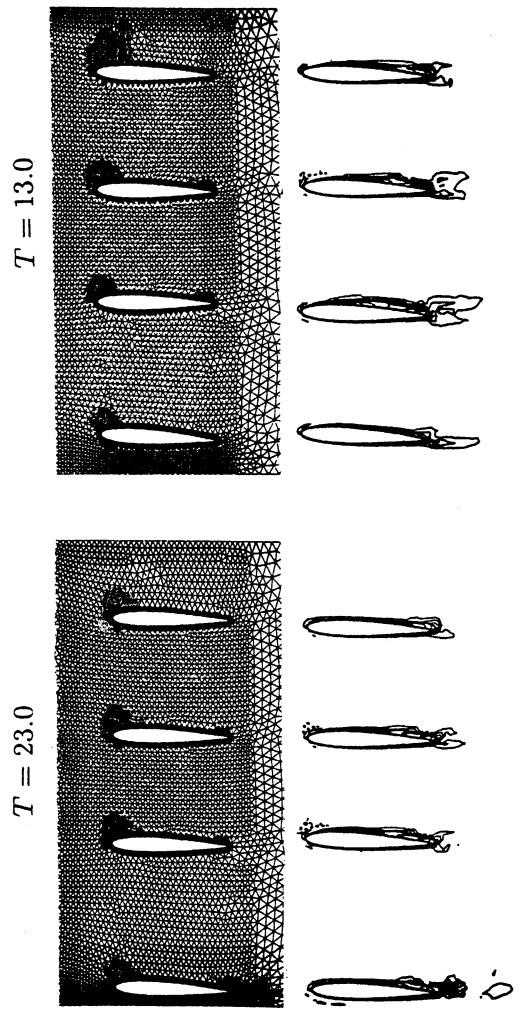


**Fig. 9 Instantaneous meshes and corresponding vorticity contours for the unstaggered NACA 0012 cascade in viscous supersonic bending flutter calculations at $M_\infty = 1.1$ and $V^* = 4.0$.**

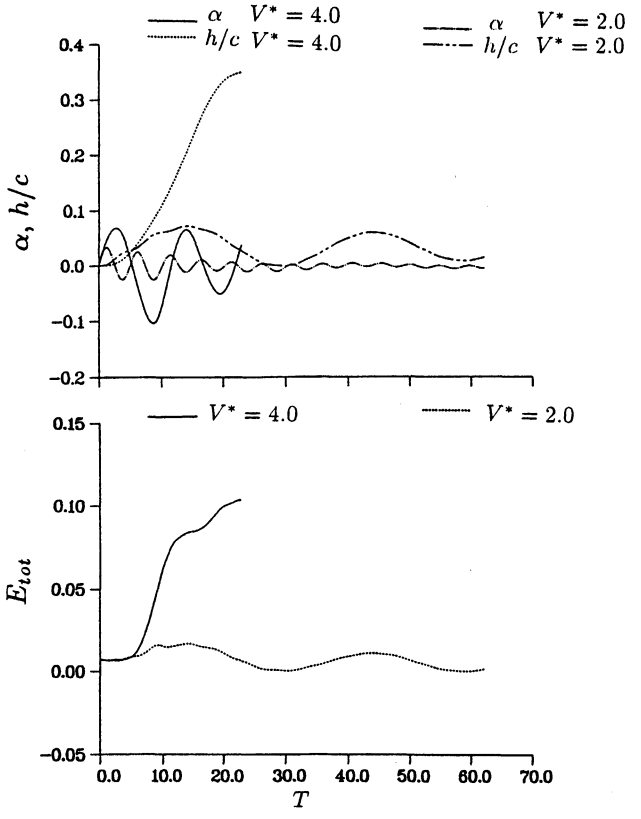


**Fig. 10 Histories of $h/c$, $\alpha$, and $E_{tot}$ for the lowest blade of an unstaggered NACA 0012 cascade in viscous supersonic bending flutter calculations at $M_\infty = 1.1$.**

set to be 1.1, 8 deg, and 1.8, respectively, the steady-state solution on a coarse mesh (Fig. 1d) is obtained first. Then, the solution-adaptive calculations with $V^* = 2.0$ and 4.0 are processed. For the case with $V^* = 4.0$, the coarse mesh is refined after $T \geq 13.0$. The instantaneous meshes and corresponding vorticity contours at $T = 13.0$ and 23.0 are plotted in Fig. 9. Unlike the subsonic stall flutter (Fig. 7), the large vortex structure is not observed. At $T = 23.0$, the lowest blade is very close to the mesh boundary. This blade motion can also be calculated from the results in Fig. 10, where the plunging displacement ($h/c$) of the lowest blade reaches the value of 0.35. Moreover, the total energy of the lowest blade progressively increases, so that the bending flutter phenomenon is triggered by the motion of lowest blade. Considering the case with $V^* = 2.0$, the time histories of $h/c$, $\alpha$, and $E_{tot}$ of the lowest blade (Fig. 10) indicate that the aeroelastic behavior of the lowest blade is dominated by bending motion, but it is stable and close to the flutter boundary. In the FFT analysis of plunging displacement (Fig. 6d), the value of reduced frequency of fundamental instability ($f_0$) is 0.0557 for the unstable case ($V^* = 4.0$; $k_h = 0.05$). From the distribution of normalized amplitude of plunging displacement, the instabilities of first ($2f_0$), second ($4f_0$), and higher harmonics exist, but the magnitudes are smaller. Therefore, the supersonic bending flutter can be determined by the fundamental instability in the present example. With regard to the case with $V^* = 2.0$ and $k_h = 0.1$, the value of fundamental frequency ($f_0$) is equal to 0.111 (Fig. 6d), which is close to the value of $k_h$. Also, the distribution of normalized amplitude of plunging displacement indicates that the aeroelastic behavior is mainly dominated by the fundamental instability. Based on the modal identification analysis and an interpolation process, the value of flutter reduced velocity is equal to 2.11.

## Conclusions

In this paper, a time-domain approach is introduced to analyze the inviscid transonic, viscous transonic, subsonic stall, and supersonic bending cascade flutter behaviors. For the present approach, the two-dimensional Euler/Navier–Stokes equations and the structural model equations, where each blade is treated as a typical section having plunging and pitching degrees of freedom, are integrated simultaneously in time. By using the explicit four-stage Runge–Kutta scheme, the structural model equations are solved to obtain the blade displacements. In the inviscid flow calculations, a solution-adaptive finite volume method with a globally dynamic mesh algorithm is adopted. To achieve the viscous flow computations, this method is extended by including a rigid-deformable dynamic mesh algorithm and a treatment of numerical viscous flux function. The Baldwin–Lomax turbulence model and two transition formulations are utilized. Comparing with the related data for two inviscid cascade problems, the reliability and suitability of the present approach are proved. Based on the time histories of blade displacements and total energy in inviscid and viscous transonic flutter calculations, the viscous effect has a damping influence on the aeroelastic behaviors. Also, the instantaneous meshes and vorticity contours indicate that the shock structure (such as the $\lambda$ shock) and related unsteady phenomena in viscous flow are different from those in inviscid flow. According to the FFT analysis of pitching displacement, the inviscid transonic flutter behavior is dominated by the fundamental instability. When the viscous transonic flutter of cascade with $V^* = 3.33$ is studied, the different value of fundamental frequency ($f_0$) is obtained, and a significant response of frequency $2f_0/3$ should be considered. For the subsonic stall flutter, the instantaneous meshes and vorticity contours clearly show the formation/convection/shedding of vorticies along the blades. When the supersonic bending flutter is studied, the big blade plunging displacement is predicted. Based on the FFT analysis of pitching or plunging displacements, the subsonic stall and supersonic bending flutter behaviors can be determined by the fundamental instability. By using the modal identification technique, the flutter reduced velocities for the present cascade problems are estimated.

## Acknowledgments

This research was supported by the National Science Council of the Republic of China under Contract NSC87-2212-E-006-087. The authors would like to acknowledge the valuable suggestions from Chingteng Hsiao, Tamsui Oxford University College, Taipei, Taiwan, Republic of China.

## References

[1]Dowell, E. H., Curtiss, H. C., Scanlan, R. H., and Sisto, F., "Aeroelasticity in Turbomachines," *A Modern Course in Aeroelasticity*, 2nd Revised and Enlarged Edition, Kluwer, Dordrecht, The Netherlands, 1989, pp. 411–442.

[2]Bakhle, M. A., Reddy, T. S. R., and Keith, T. G., Jr., "Time Domain Flutter Analysis of Cascades Using a Full-Potential Solver," *AIAA Journal*, Vol. 30, No. 1, 1992, pp. 163–170.

[3]Reddy, T. S. R., Bakhle, M. A., Huff, D. L., and Swafford, T. W., "Flutter Analysis of Cascades Using a Two Dimensional Euler Solver," AIAA Paper 91-1681, June 1991.

[4]Bendiksen, O. O., and Hsiao, C., "New Computational Method for Aeroelastic Problems in Turbomachines, Part II," Univ. of California, Rept. ENG-93-14, Los Angeles, CA, April 1993.

[5]Sisto, F., Thangam, S., and Abdel-Rahim, A., "Computational Prediction of Stall Flutter in Cascaded Airfoils," *AIAA Journal*, Vol. 29, No. 7, 1991, pp. 1161–1167.

[6]Boschitsch, A. H., and Quackenbush, T. R., "Adaptive Grid Computation of Transonic Flows Through Cascades and Investigation of Chordwise Bending upon Aeroelastic Response," AIAA Paper 94-0145, Jan. 1994.

[7]Hwang, C. J., and Fang, J. M., "Solution-Adaptive Approach for Unsteady Flow Calculations on Quadrilateral-Triangular Meshes," AIAA Paper 95-1723, June 1995.

[8]Hwang, C. J., and Yang, S. Y., "Viscous Solutions for Transonic Oscillating Cascade Flows Using Dynamic Quadrilateral-Triangular Meshes," American Society of Mechanical Engineers, Paper 94-GT-21, June 1994.

[9]Abu-Ghannam, B. J., and Shaw, R., "Natural Transition of Boundary Layers—The Effects of Turbulence, Pressure Gradient, and Flow History," *Journal Mechanical Engineering Science*, Vol. 22, No. 5, 1980, pp. 213–228.

[10]Mayle, R. E., "The Role of Laminar-Turbulent Transition in Gas Turbine Engines," *Journal of Turbomachinery*, Vol. 113, No. 4, 1991, pp. 509–537.

[11]Baldwin, B. S., and Lomax, H., "Thin Layer Approximation and Algebraic Model for Separated Turbulent Flows," AIAA Paper 78-257, Jan. 1978.

[12]Giles, M. B., "Nonreflecting Boundary Conditions for Euler Equation Calculations," *AIAA Journal*, Vol. 28, No. 12, 1990, pp. 2050–2058.

[13]Bennett, R. M., and Desmarais, R. N., "Curve Fitting of Aeroelastic Transient Response Data with Exponential Functions," *Flutter Testing Techniques*, NASA SP-415, May 1975, pp. 43–58.